Supplementary Information

Triple-helix molecular switch photoelectrochemical biosensor for ultrasensitive microRNA detection based on position-controllable CdS//CdTe signal enhancing and switching

Wenchao Geng,[a] and Ruiying Yang*[,a,b]

[a]State Key Laboratory of Chemo/Biosensing and Chemometrics, College of Chemistry and Chemical Engineering, Hunan University, Changsha, 410082, China

[b]College of Public Health, Zhengzhou University, Zhengzhou, 450001, China

List of Contents:

1. Materials and reagents

The ITO slices were provided by Zhuhai Kaivo Electronic Components Co., Ltd, China. Tris-(2-carboxyethyl) phosphine hydrochloride (TCEP), and Bovine serum albumin (BSA) were obtained from Sigma-Aldrich (USA). Nt.BsmAI nicking endonuclease (Nt.BsmAI) was purchased from New England Biotechnology Co., Ltd. (Beijing, China). SH-β-cyclodextrin (β-CD) was obtained from Shandong Binzhou Zhiyuan Bio-Technology Co. Ltd., China. Cadmium nitrate ($Cd(NO_3)_2 \cdot 4H_2O$), sodium tellurite (Na_2TeO_3), sodium sulfide ($Na_2S \cdot 9H_2O$), trisodium citrate, sodium acetate (NaAc), potassium borohydride (KBH_4), ascorbic acid (AA), silver nitrate ($AgNO_3$), and ethylene glycol were all provided by Sinopharm Chemical Reagent Co., Ltd. Cetyltrimethylammonium bromide (CTAB) was gotten from Hefei Bomei Biotechnology co. Ltd. Cetyltrimethylammonium chloride (CTAC) was bought from TCI Industrial Development co. Ltd. 3-Mercaptopropionic acid (MPA) was obtained from Alfa Aesar. Carboxyl-modified magnetic beads were obtained from Tianjin Base Line Chromatographic Technology Development Center. All oligonucleotide sequences (Table S1) in this work were provided by Sangon Biotech Co., Ltd. (Shanghai, China). Ultrapure water was purified by a Milli-Q purification system (Millipore Corp., Bedford, MA).

Table S1. Sequences of oligonucleotides used in this work.

Oligonucleotides	Sequences (from 5' to 3')
Walker	HS-$(CH_2)_6$-TTT TTT TGT ACT TGA TAC ATC TGC CAT GTC TCC GAG ACA GGT AAA GAT GGC TTT TTT

Protecting	AAA AAA GCC ATC TTT ACC AGA CAG TGT TA
Support	HS-$(CH_2)_6$-TTT TTT AAC GTC TCG GAG AGA GCT CCT CTC TCG AGA GAG
RhB-DNA1	HS-$(CH_2)_6$-GCA GTG AGA GAG GAG ACT GC-$(CH_2)_6$-RhB
DNA2	NH_2-$(CH_2)_6$-CTCTCTCTTTTTTTTTTCTCTCTC-$(CH_2)_6$-NH_2
miRNA-141	UAACACUGUCUGGUAAAGAUGG
miRNA-21	UAGCUUAUCAGACUGAUGUUGA
miRNA-155	UUAAUGCUAAUCGUGAUAGGGGU

2. Apparatus

The morphology of the synthesized materials was characterizated by transmission electron microscopy (TEM, JEM-2100F, Japan). The UV-vis spectra were obtained using a UV-2500 UV-vis spectrophotometer (LabTech). A xenon lamp of 300W (PLS-SXE) equipped with a 420 nm filter was acted as the excitation source. Photoelectrochemical (PEC) and electrochemical tests were performed on a CHI 660D electrochemical working station with a three-electrode system: a modified ITO electrode (diameter, 5.6 mm) as the working electrode, a platinum wire as the counter electrode, and a saturated calomel electrode (SCE) as the reference electrode.

3. Preparation of Au@Ag core–shell NBs

The Au nanorods (NRs) were synthesized according to the previously reported paper.[1] Specically, the Au seed solution was prepared by mixing $HAuCl_4$ (0.01 M, 0.25 mL) and CTAB (0.1 M, 10 mL) in a 15 mL plastic tube. Then, An ice-cold $NaBH_4$ solution (0.01 M, 0.6 mL) was injected quickly into the mixture solution, followed by rapid inversion for 1 min. The seed solution was kept at room temperature for at least 2 h before use. To grow Au NRs, $HAuCl_4$ (0.01 M, 5 mL) and $AgNO_3$ (0.01 M, 1 mL) were mixed with CTAB (0.1 M, 95 mL) in a 150 mL plastic tube, followed by the addition of AA (0.1 M, 0.55 mL). Finally, the seed solution (0.12 mL) was injected into the growth solution. The solution was gently mixed for 20 s and left undisturbed at room temperature for at least 12 h before use. Then, the Au NRs were centrifuged and redispersed in water.

The Au@Ag core–shell nanocuboids (NBs) were prepared as reported literature with slight modification.[2] In briefly, the above Au NRs solution (50 mL) was centrifuged and dispersed in CTAC aqueous solution (0.08 M, 50 mL). The solution was kept at room temperature for at least 12 h to make sure the CTAB completely replaced by CTAC. Then $AgNO_3$ solution (0.01 M, 5 mL) was added into the above solution under agitation, followed by the addition of AA solution (0.1 M, 2.5 mL). The resultant solutions were kept in an isothermal oven at 65 °C for 3 h. Then the abtained Au@Ag core–shell NBs were centrifuged two times and redispersed in water.

4. Preparation of CdS QDs and RhB-DNA1-CdS

0.1 M Na_2S (22 mL) methanol/water mixture (1:1, v/v) was added into of 0.1 M $Cd(NO_3)_2$ (20 mL) methanol solution under stirring for 2 h. Then the synthetic products were centrifuged and washed. Finally, the obtained CdS quantum dots (QDs) were dispersed in 20 mL water and irradiated by infrared lamp over 2 h.[3] For the preparation of CdS QDs-labeled RhB-DNA1 (RhB-DNA1-CdS), 50 μL of 10 μM RhB-DNA1 and 10 μL of 10 mM TCEP were mixed and incubated for 1 h at 37 ºC to reduce disulfide bonds. Then 1 mL of CdS QDs (pH 7.4) was added into the above solution, and which was incubated for 16 h at room temperature under gentle shaking and dark environment. The resultant solution was centrifuged for 10 min at 8000 rpm and 4 ºC.

5. Preparation of CdTe QDs and DNA2-CdTe

The p-type CdTe QDs are fabricated by the solution method.[4,5] In brief, $Cd(NO_3)_2$ (236 mg), trisodium citrate (400 mg) and MPA (110 μL) were poured into 100 mL ultrapure H_2O. Then, the pH of the solution was adjusted to 10.5 by NaOH solution (1.0 M). Subsequently, KBH_4 (100 mg) of and Na_2TeO_3 (45 mg) were successively joined, and the mixture was heated to 100 °C and refluxed for 1 h under N_2 protection, and the CdTe-COOH QDs solution was achieved. Then, 10 μM DNA2 (10 μL) and CdTe QDs (100 μL) were mixed. DNA2 were linked to CdTe QDs via the EDC coupling reaction with 2.5 μL of EDC (400 mM) and 100 mM of NHS (2.5 μL) for 1 h at 37 °C.

6. Preparation of transformational DNAs

First, walker DNA (10 μM, 20 μL) and protecting DNA (10 μM, 40 μL) were annealed at 95 °C for 5 min, and then naturally cooled to obtain (double-stranded DNAs) dsDNAs. Afterwards, dsDNAs (20 μL) and support DNA (50 μM, 20 μL) were blended in PBS (40 μL, 10 mM TCEP, pH 7.4) for 60 min to reduce disulfide bonds, followed by the addition of Fe_3O_4@Au NPs (10 mg·mL^{-1}, 20 μL). Then the mixture was slightly shaken for 16 h at 4 °C. Afterward, by using BSA to block the nonspecific adsorption sites, the Fe_3O_4@Au-dsDNAs were obtained by magnetic separation and washing. In presence of different-concentration miRNA-141 (50 μL), walker probes will be released and further hybridized with support probes for 1 h at 37 °C. After that, 10 U Nt.BsmAI were appended and maintained 2 h at 37 °C to cut the recognition sites and generate transformational DNAs. Finally, numerous transformational DNAs were achieved through magnetic separation.

7. Fabrication of the PEC biosensor and PEC assay

Before use, ITO electrodes were sequentially ultrasonically treated with acetone, 1 M NaOH in ethanol/water mixture (v/v, 1:1), and H_2O. Subsequently, 20 μL Au@Ag core–shell NBs solution was dropped onto the cleaned ITO electrode surface. After drying in air, the ITO/Au@Ag electrode was obtained. Then, the ITO/Au@Ag electrode was immersed in 3 mM β-CD solution (0.1 M PBS, pH 7.4) for 12 h. Afterward, the ITO/Au@Ag/β-CD electrode was incubated with 20 μL of 1 μM RhB-DNA1-CdS solution for 4 h to assemble RhB-DNA1-CdS on the electrode via the host-guest interaction between β-CD and RhB. To block the nonspecific sites of the

electrode surface, the obtained electrode was covered with 20 μL of 0.5% wt BSA and incubated for 1 h at room temperature. Subsequently, the electrode was further reacted with DNA2-CdTe (20 μL) for 90 min to form the triple-helix molecular conformation. After that, the above transformational DNAs (20 μL), which linearly correlated with target miRNA-141, were coated onto the resulting ITO/Au@Ag/β-CD/RhB-DNA1-CdS/BSA/DNA2-CdTe electrode for 120 min to adjust the location between CdS and CdTe, and a significantly photocurrent-polarity change from cathodic photocurrent to anodic photocurrent was obtained because of the well-matched energy levels between CdS and CdTe. Finally, PEC assay of the developed biosensor was performed in Tris–HCl solution (0.1 M, pH 7.4) containing AA (0.1 M) at 0 V.

8. The effect of the Au@Ag NBs on the photocurrent of ITO/CdS electrode

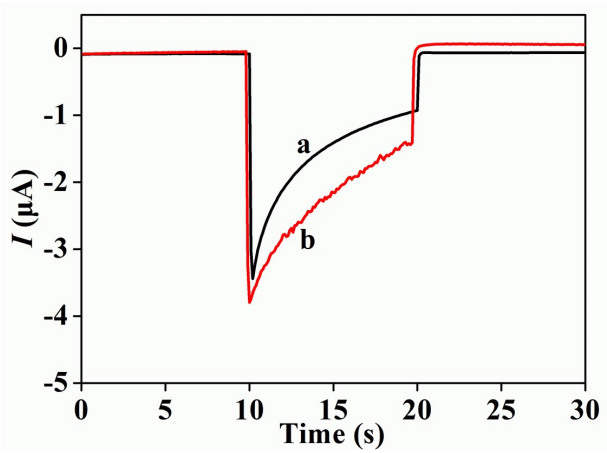

Fig. S1 Photocurrent responses of (a) ITO/CdTe and ITO/Au@Ag/CdS electrodes.

To investigate the advantage of Au@Ag core–shell NBs to the photocurrent of CdS, several control experiments were carried out (Fig. S1). It is noted that an increased photocurrent of ITO/Au@Ag/CdS electrode (curve b) can be observed

compared with ITO/CdS electrode (curve a), which may be because Au@Ag core–shell NBs with good conductivity, as an electron mediator, can facilitate electron transfer and suppress recombination of electron−hole pairs.

9. The effect of the RhB on the photocurrent of ITO/CdS electrode

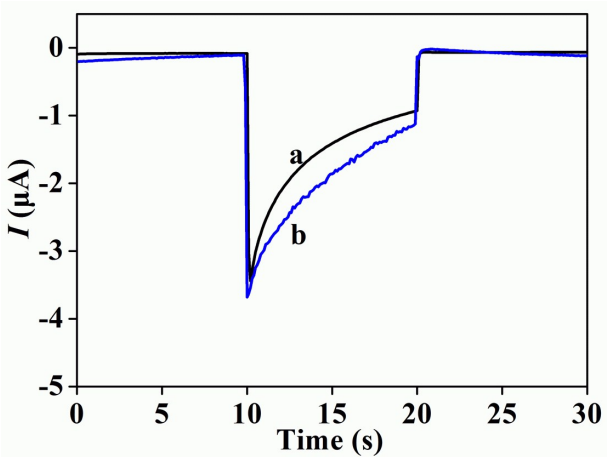

Fig. S2 Photocurrent responses of (a) ITO/CdTe and ITO/RhB/CdS electrodes.

To investigate the sensitization efficiency of RhB towards CdS, several control experiments were carried out (Fig. S2). It is noted that the ITO/RhB/CdS electrode (curve b) generates a slightly bigger photocurrent than that of ITO/CdS electrode (curve a), according to the fact that the sensitization efficiency of RhB may promote charge separation of CdS, leading to a strong cathodic photocurrent.[6]

10. Electrochemical properties of CdS and CdTe QDs

To observe the electrochemical properties of CdS and CdTe, the conduction band (CB) and the valence band (VB) of CdS and CdTe were investigated by electrochemical method (Fig. S3).[7,8] The results show that CdS has a CB edge at -

1.22 V and a VB edge at 1.05 V, and CdTe has a CB edge at -1.47 V and a VB edge at 0.57 V vs. SCE. In other words, the CB and VB potentials of CdS are -0.98 and 1.29 V, and those of CdTe are -1.23 and 0.81 V vs. the normal hydrogen electrode (NHE), respectively. These values will be useful for understanding the PEC behaviors of the designed CdS//CdTe system.

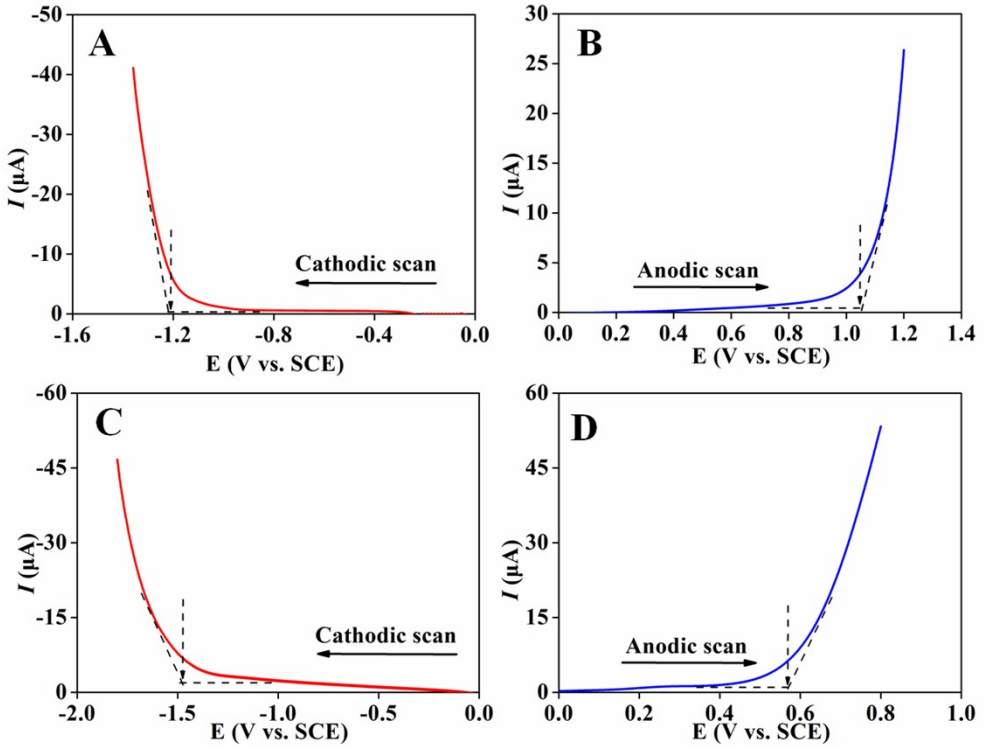

Fig. S3 Cathodic and anodic linear potential scans for determining the conduction (CB) and valence band edge (VB) of CdS (A, B) and CdTe (C, D) in N_2-saturated Tris-HCl solution (0.1 M, pH 7.4).

11. The effect of the dissolved oxygen on the photocurrent of ITO/CdS electrode

To investigate the conformation of O_2•- production, several control experiments

were carried out (Fig. S4). Fig. S4 shows the effect of the dissolved oxygen on the photocurrent of ITO/CdS electrode. It is noted that the photocurrent of ITO/CdS electrode in air-saturated solution (curve a) is much larger than that in N_2-saturated solution (curve b). This phenomenon may demonstrate that dissolved oxygen as an electron acceptor can scavenge photo-generated electrons from the CdS-based PEC system to produce O_2•- and greatly enhance charge separation of semiconductors, resulting in the promoted photocurrent.[9,10]

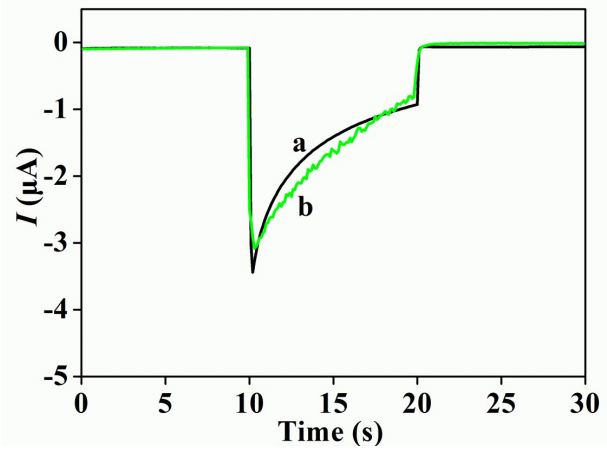

Fig. S4 (C) Photocurrent responses of the ITO/CdS electrode in the air-saturated (a) and N_2-saturated (b) Tris−HCl solution (0.1 M, pH 7.4) containing 0.1 M AA.

12. Position-controllable CdS//CdTe signal enhancing and switching mechanism

According to the results shown in Fig. 2 and Fig. S3-S4, the possible electron-transfer mechanisms of the ITO/CdS/CdTe and ITO/CdTe/CdS electrodes (Scheme S1) are as follows: in case of ITO/CdS/CdTe electrode (Scheme S1B), under visible light excitation, the electrons of CdTe is excited from VB (0.81 V) to CB (-1.23 V), and further transfer from the CB of CdTe to the CB (-0.98 V) of CdS due to the well-

match energy level between CdTe and CdS. Then, the electrons on the CB of CdS (-0.98 V) transfer to the ITO electrode, where AA is chosen as electron donor to oxidize photo-generated holes to reduce the recombination of photo-generated electron-hole pairs, resulting in an effectively improved electron transfer capability. Thus, a large anodic photocurrent is achieved and the photocurrent-direction is switched compared with ITO/CdS electrode (Scheme S1A). For the ITO/CdTe/CdS electrode (Scheme S1D), the photo-generated electrons on the CB of CdTe (-1.23 V) transfer to the CB (-0.98 V) of CdS, and then are further excited for the electrochemical reduction of O_2 (electron acceptors) in the electrolyte. Meanwhile, AA can effectively be oxidized by photo-generated holes to reduce the recombination of photo-generated electron-hole pairs. Thus, an enhanced cathodic photocurrent is obtained compared with ITO/CdTe electrode (Scheme S1C).[9-12] Obviously, such an interesting position-controllable CdS//CdTe signal enhancing and switching effect will be very useful for the proposed PEC biosensing strategy (Scheme 1).

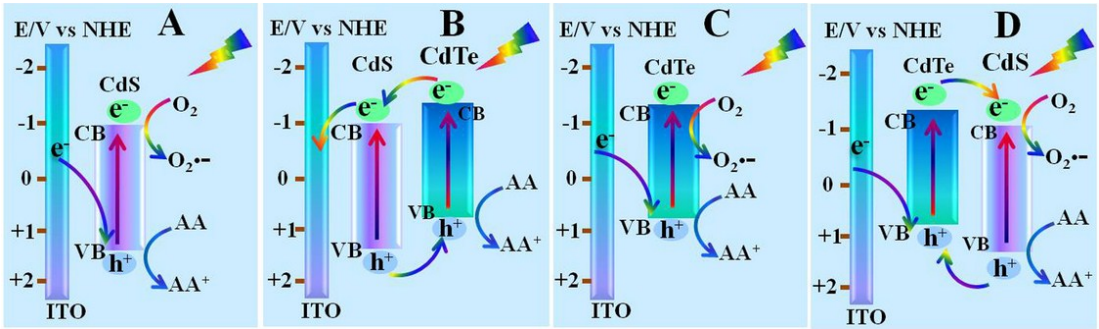

Scheme S1. The possible electron-transfer mechanism of (A) ITO/CdS, (B) ITO/CdS/CdTe, (C) ITO/CdTe, and (B) ITO/CdTe/CdS electrodes.

13. Optimization of experimental conditions

To achieve the excellent performance of the developed PEC biosensor for

miRNA-141 detection, the concentration of RhB-DNA1-CdS and cleaving time of Nt.BsmAI on the photocurrent responses of the modified electrodes were investigated. As shown in Fig. S5A, with the increase of RhB-DNA1-CdS concentration, the cathodic photocurrent increases and reaches a plateau at 90 min, implying the saturated immobilization of RhB-DNA1-CdS. Thus, 1.0 μM is served as the optimum RhB-DNA1-CdS concentration. Fig. S5B shows the effect of the cleaving time of Nt.BsmAI on the PEC biosensor. When the incubation time is prolonged, more transformational DNAs generate, leading to the introduction of more DNA2-CdTe to the biosensing platform. The anodic photocurrent increases and achieves a plateau at 120 min. Thus, the optimum cleaving time of Nt.BsmAI in this work is 120 min.

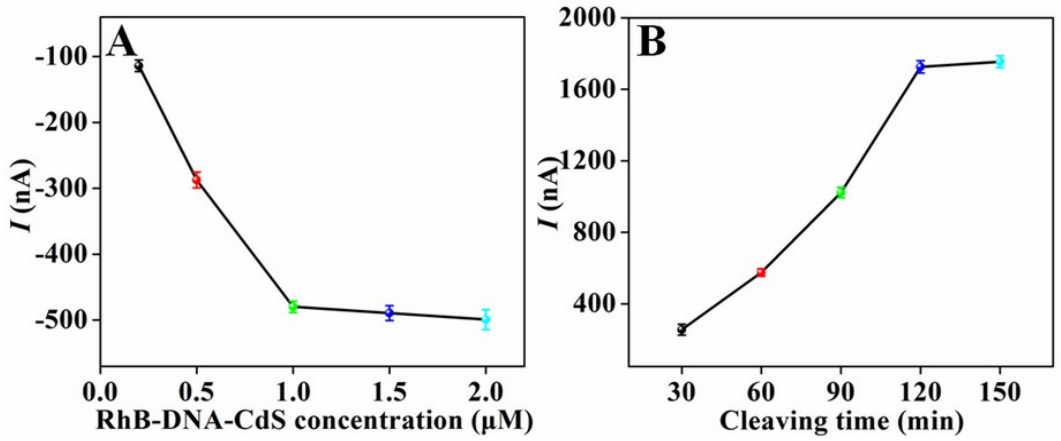

Fig. S5 The effects of the concentration of RhB-DNA1-CdS (A), and cleaving time of Nt.BsmAI (B) on the photocurrent responses of the modified electrodes.

14. Comparison of various methods for miRNA-141 detection

Table S2. Comparison of various methods for miRNA-141 detection

Mehods	signal mode	Linear range	LOD	Ref.
ECL	Distance-controllable signal quenching and enhancing	10 fM~100 pM	3.3 fM	13
ECL	Near-zero background noise	50 aM~50 pM	17 aM	14
ECL	Faraday cage-type strategy	0.1 fM~1 pM	0.03 fM	15
FL	Non-enzymatic target recycling amplification	0.1 pM~10 nM	80 fM	16
PEC	Electron-transfer tunneling distance regulation	0.25 fM~25 pM	83.3 aM	17
PEC	G−wire-enhanced strategy	10 aM~1nM	4.8 aM	18
PEC	Signal amplification of click chemistry	0.1 fM~0.5 nM	27 aM	19
PEC	Energy transfer	1 fM~10 pM	0.5 fM	20
PEC	Position-controllable signal enhancing and switching	5 aM~100 fM	1.3 aM	Our work

15. **Selectivity, reproducibility, and stability**

To investigate the selectivity of the proposed PEC biosensing system, a contrast experiment was performed by incubating the sensor with interferences including 500 fM miRNA-155 and miRNA-21. As shown in Fig. S6, compared with the blank solution, the photocurrent direction is no change for the interferences. Nevertheless, the cathodic photocurrent obtained from the target miRNA-141 (5 fM) is switched to

a big anodic photocurrent, due to the target-induced relative position adjustion of CdS//CdTe and electron-transfer tunneling regulation of the biosensor. This implies that the proposed strategy has an outstanding selectivity and can avoid the possible false positive or negative impact.

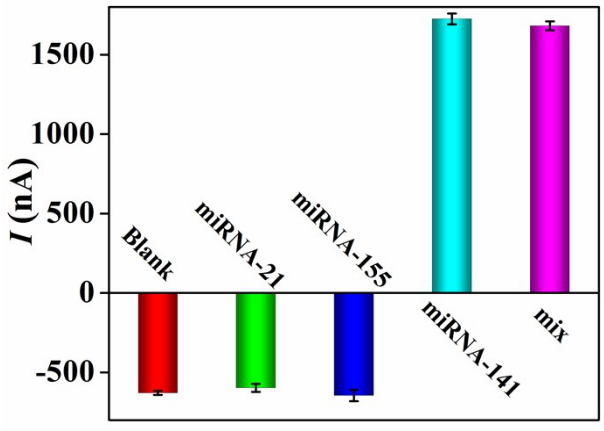

Fig. S6. Selectivity of the developed PEC biosensor. The miRNA-141 concentration, 5 fM; the concentrations of other proteins (miRNA-155 and miRNA-21), 500 fM.

The reproducibility of the proposed PEC biosensor is verified by the relative standard deviation (RSD). The resultant electrode incubated with 5 fM miRNA-141 is repeatedly tested five times, giving a RSD of 3.8%. Also, the stability of the system was surveyed. Three independent experiments indicate that the electrode retains about 95.9% of its initial response toward miRNA-141 after its storage in the refrigerator at 4 °C over 15 days. The results suggest the good reproducibility and stability of the developed PEC biosensor.

16. Recovery test

To evaluate the applicability and reliability of the proposed PEC system in complex biological system, the recovery tests were performed for different

concentrations of miRNA-141 (5, 50, 100, and 500 aM) added in the 10−fold diluted (10 mM PBS, pH 7.4) human serum samples, giving the recoveries of 97%, 100.6%, 98.7%, and 101.7%, respectively (Table S3). These results reveal that the proposed PEC biosensor is satisfactory and has potential application in the detection of miRNA-141 in complex biological samples.

Table S3. Recovery tests of miRNA-141 in the human serum samples.

Sample	Added (aM)	Found (aM)	Recovery (%)
1	1	0.97±0.11	97
2	5	5.03±0.28	100.6
3	10	9.87±0.54	98.7
4	50	50.83±1.02	101.7

17. Characterization of Au NRs and Au@Ag NBs

The TEM image of the as-prepared Au NRs was characterized in Fig. S7A. From Fig. S7A, it is noted that the Au NRs have uniform size distributions. Moreover, Au NRs (Fig. S7C) shows two characteristic absorption peaks at 515 nm and 750 nm.[21] After the Au nanorod core is fully enwrapped with a uniform Ag shell, the TEM image of the abtained Au@Ag NBs (Fig. S7B) reveals the four faces at the side of the Au nanorod are rectangular, and the two faces at the top of the Au nanorod are square. Furthermore, Au@Ag NBs (Fig. S7D) have four characteristic absorption peaks at 516 nm, 451 nm, 387 nm and 347 nm, respectively, demonstrating the successful preparation of the Au@Ag NBs.[2]

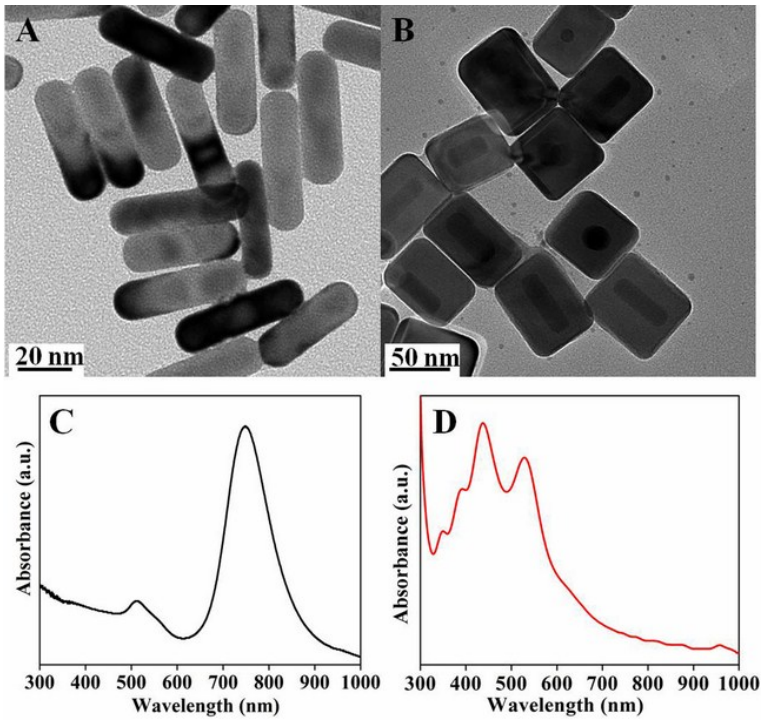

Fig. S7 TEM images of (A) Au NRs and (B) Au@Ag NBs, UV-Vis absorption spectra of (C) Au NRs and (D) Au@Ag NBs.

18. PAGE analysis

The 13% PAGE is carried out to corroborate the interactions among these DNA sequences. As shown in Fig. S8, a single distinct band is observed, corresponding to walker DNA (lane 1). Then, multiple separate bands are observed from the mixture of walker DNA, support DNA, protecting DNA and miRNA-141 (lane 2). As protecting DNA firstly pairs with walker DNA, miRNA-141 is added to pair with protecting probe for releasing of walker DNA which further pairs with support DNA. In addition, there may be a very small number of bases in the hybridized dsDNA of walker-support DNA and walker-protecting DNA, the top band is corresponded to them, and the bottom band is corresponded to the hybridized dsDNA of protecting probe and

miRNA-141. Subsequently, the walker DNA is mixed with support DNA, and a clear band at high position is observed (lane 3), indicating the formation of walker-support dsDNA. Then 10 U Nt.BsmAI is added into the above mixture, resulting in the appearance of multiple bands (lane 4). The band at the low position corresponded to the single stranded DNA (transformational DNA) releases from the walker-support dsDNA. Besides, the band at the high position is similar with the band of walker probe in Lane 1, indicating the successful releasing of walker probe. The above results confirm the interactions among these DNA sequences.

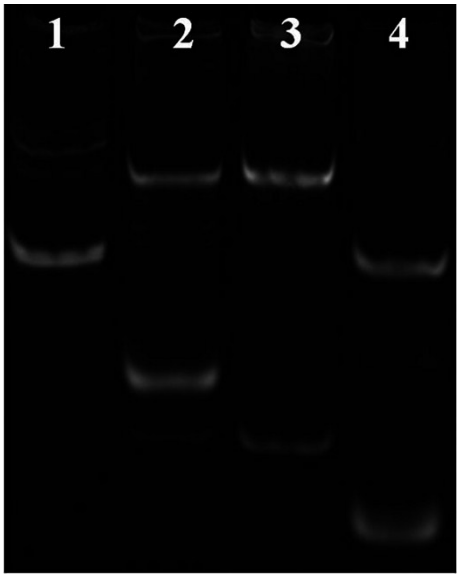

Fig. S8 13% PAGE of different samples. Lane 1: 2 μM walker DNA; Lane 2: mixture of 2 μM walker DNA, 2 μM protecting DNA, 2 μM support DNA and 2 μM target miRNA-141; Lane 3: mixture of 2 μM walker DNA and 2 μM support DNA; Lane 4: mixture of 2 μM walker DNA and 2 μM support DNA with 10 U Nt.BsmAI.

19. References

[1] Z. Y. Bao, D. Y. Lei, R. B. Jiang, X. Liu, J. Y. Dai, J. F. Wang, H. L. W. Chan and Y. H. Tsang, *Nanoscale,* 2014, **6**, 9063–9070

[2] R. B. Jiang, H. J. Chen, L. Shao, Q. Li and J. F Wang, *Adv. Mater.* 2012, **24**, OP200–OP207.

[3] F. Wang , X. Q. Liu and Itamar Willner, *Adv. Mater.* 2013, **25**, 349–377.

[4] Y. M. Li, L. X. Meng, K. Zou, X. H. Zhang and J. H. Chen, *J. Electroanal. Chem.* 829, 51–58.

[5] Q.Wang, Y. F. Ruan, W. W. Zhao, P. Lin, J. J. Xu and H. Y. Chen, *Anal. Chem.* 2018, **90**, 3759-3765.

[6] T. Iwamoto, Y. Ogawa, L. Sun, M. S. White, E. D. Glowacki, M. C. Scharber, N. S. Sariciftci, K. Manseki, T. Sugiura, and T. Yoshida, *J. Phys. Chem. C* 2014, **118**, 16581–16590.

[7] R. Y. Yang, K. Zou, X. H. Zhang, C. C. Du and J. H. Chen, *Biosens. Bioelectron.* 2019, **132***,* 55–61.

[8] T. F. Yeh, S. J. Chen, C. S. Yeh and H. *J.* Teng, *Phys. Chem. C.* 2013, **117**, 6516−6524.

[9] G. Y. Zhang, Y. H. Zhuang, D. Shan, G. F. Su, S. Cosnier and X. J. Zhang, *Anal. Chem.* 2016, **88,** 11207–11212.

[10] Q. Hao, P. Wang, X. Y. Ma, M. Q. Su, J. P. Lei and H. X. Ju, *Electrochemistry Communications.* 2012, **21,** 39–41.

[11] C. Ye, M. Q. Wang, H. Q. Luo and N. B. Li, *Anal. Chem.* 2017, **89,** 11697-11702.

[12] R. Y. Yang, Y. M. Li, K. Zou, L. X. Meng, X. H. Zhang and J. H. Chen, *Chem. Commun.* 2018, **54,** 4830–4833.

[13] Z. Q. Xu, L. L. Liao, Y. Q. Chai, H. J. Wang and R. Yuan, *Anal. Chem.* 2017, **89**,

8282−8287.

[14] M. J. Li, C. Xiong, Y. N. Zheng, W. B. Liang, R. Yuan and Y. Q. Chai, *Anal. Chem.* 2018, **90**, 8211−8216.

[15] J. Lu, L. Wu, Y. F. Hu, S. Wang and Z. Y. Guo, *Biosens. Bioelectron.* 2018, **109**, 13–19.

[16] X. Li, D. X. Li, W. J. Zhou, Y. Q. Chai, R. Yuan and Y. Xiang, *Chem. Commun.* 2015, **51**, 11084−11087.

[17] Y. N. Zheng, W. B. Liang, C. Y. Xiong, Y. Zhuo, Y. Q. Chai and R. Yuan, *Anal. Chem.* 2017, **89**, 9445−9451.

[18] C. Ye, M. Q.Wang, H. Q. Luo and N. B. Li, *Anal. Chem.* 2017, **89***,* 11697−11702.

[19] C. Ye, M. Q. Wang, Z. F. Gao, Y. Zhang, J. L. Lei, H. Q. Luo and N. B. Li, *Anal. Chem.* 2016, **88**, 11444−11449.

[20] N. Zhang, X. M. Shi, H. Q. Guo, X. Z. Zhao, W. W. Zhao, J. J. Xu and H. Y. Chen, *Anal. Chem.* 2018, **90**, 11892–11898.

[21] Z. Y. Bao, W. Zhang, Y. L. Zhang, J. J. He, J. Y. Dai, C. T. Yeung, G. L. Law and D. Y. Lei, *Angew. Chem. Int. Ed.* 2016, **55**, 1–7.